Pergamon

PII: S0967-0645(96)00047-1

Deep-Sea Research II, Vol. 43, No. 7-8, pp. 1575-1600, 1996

0967-0645/96 $15.00 + 0.00

Assessment of Georges Bank recirculation from Eulerian current observations in the Great South Channel

J. P. MANNING* and R. C. BEARDSLEY†

(*Received* 10 *December* 1994; *in revised form* 29 *November* 1995; *accepted* 6 *May* 1996)

Abstract—Twenty Vector Averaging Current Meters (VACMs) were deployed at various depths in the vicinity of the Great South Channel during several experiments conducted between 1976 and 1986 (average record length ~5 months). Since little more than mean current vectors from some records has been reported previously, a basic description of the flow field is presented here. With at least one current record occurring in every month of the year, the hypothesis of increased subtidal flow around Georges Bank during the stratified season is supported. Anemometer data obtained at nearby NOAA environmental buoys and the Nantucket Lightship are used to estimate wind stress, the primary forcing in the well-mixed season. Empirical modes of current structure demonstrate the spatial structure and the seasonal variability of wind and density-driven dynamics in this region. When averaged over a few months, the northward transport through the Great South Channel (fall mean ~0.095 Sv) is small compared to the westward transport along the southern flank of Georges Bank (fall mean ~0.421 Sv), but the subtidal variability of the Great South Channel transport is highly energetic, with a standard deviation (~0.11 Sv) greater than the mean, indicating that large reversals in transport can occur over a few days. Copyright © 1996 Elsevier Science Ltd

INTRODUCTION

While studies as far back as the classic observations of Bigelow (1927) and the more recent reviews by Bumpus (1976) and Butman and Beardsley (1987a, 1987b) have documented a clockwise recirculation gyre around Georges Bank, the degree to which it occurs, its variability, and especially its biological significance are still unknown. The hypotheses that this recirculation phenomenon is critical to the survival of fish eggs and larvae is still under investigation.

The Bureau of Land Management sponsored a large-scale monitoring program in the late 1970s. Most of the observations and subsequent analysis focused on the southern flank region of Georges Bank (Butman *et al.*, 1982, 1983; Noble *et al.*, 1985; Butman and Beardsley, 1987a, 1987b) to help assess the impact of offshore drilling proposed for that area. A few current meter moorings were deployed by the United States Geological Survey (USGS) and Woods Hole Oceanographic Institution (WHOI) in the vicinity of the Great South Channel (GSC) on the southwestern flank of Georges Bank, but, given the limited number of sites and the lack of summertime observations, very little evidence was available to quantify the recirculation.

Several years later, in response to increased interest in the physical oceanographic

* United States Department of Commerce, National Oceanic and Atmopheric Administration, National Marine Fisheries Service, Woods Hole, MA 02543, U.S.A.

† Woods Hole Oceanographic Institution, Woods Hole, MA 02543, U.S.A.

processes affecting the early life stages of economically important fish species, the National Oceanic Atmospheric Administration's National Marine Fisheries Service (NMFS) sponsored seven-month deployments of several current meter moorings during the spring/summer periods in the GSC region in 1985 and 1986. The combination of all these datasets (USGS, WHOI, and NMFS) provide a full year of observations.

Since little more than mean current vectors from some records has been reported elsewhere, this paper presents a basic description of the flow field based on the combined current meter records from the GSC region and begins an investigation of wind and density-driven dynamics relative to recirculation around Georges Bank. First, the moored arrays are described. This is followed by a description of the methods taken to correct biofouled records, the tidal current statistics, the subtidal current statistics, and the monthly mean flow fields. Next, the coherence and phase between (i) different current meter locations and (ii) the wind and current are discussed. Principal component analysis is presented in the case of the two longest deployments in an attempt to distinguish between wind and density-driven components of flow. Finally, transport estimates are presented to investigate recirculation around Georges Bank.

DATA

A single near-bottom Vector Averaging Current Meter (VACM) was deployed by the USGS in the middle of the Great South Channel (Site N, Fig. 1a) from March 1976 to July 1976, and then again from December 1979 to May 1980. A three-element array of VACMs was deployed by WHOI with USGS support between August 1978 and March 1979. This array consisted of three instrumented subsurface moorings (Sites M, N, and O) supporting one or two VACMs, and a surface mooring at each site that contained a single VACM at 10 m. At each of the three mooring locations, the surface and subsurface moorings were separated by about 200 m. A second surface mooring without instrumentation was deployed at each site so that the subsurface mooring was bracketed by two lighted, radar-reflecting surface buoys.

NMFS deployed an array of VACMs from April to November 1985 (Fig. 1b). Sites 1 and 4 consisted of a single surface mooring with a VACM at 10 m. The mooring configuration at the other sites (2, 3, 5, 6, and 7) included an instrumented subsurface mooring and a surface moorings instrumented with a VACM at 10 m. A second uninstrumented surface buoy also was deployed at each site. In April 1986, moorings were deployed again at sites 2, 3, 5, and 6 by NMFS. Site 3 contained a surface and subsurface mooring, while single surface moorings with VACMs at 10 m were deployed at sites 2, 5, and 6.

The geographic location, water and instrument depths, start/stop times, temperature and current statistics for all good data are given in Table 1 along with a note describing the problems encountered in recovering and processing records. The time period of good data and the water column depth of each instrument is depicted in Fig. 2.

Seventeen years of wind data collected in the vicinity of the Great South Channel were obtained from the NOAA National Data Buoy Center (NDBC). Three-hourly anemometer records from the Nantucket Lightship (40°30′N, 69°16.8′W; 1976–1977) and hourly wind data from NOAA Environmental Buoys no. 44003 (40°48′N, 68°30′W; 1978–1983) and no. 44008 (40°30′N, 69°30′W; 1984–1992) provide a nearly continuous time-series of wind for all the current meter deployment periods. These data were used to compute wind statistics (Table 2).

Table 1. Current meter position, start/stop time of good data, depth, and statistical information

Station	Position		Time		No. of Days	Water Depth (m)	Instr. Depth (m)	Temperature (°C)				East (cm s^{-1})				North (cm s^{-1})				Speed (cm s^{-1})		
	Latitude	Longitude	Start	Stop				Mean	Std	Min	Max	Mean	Std	Min	Max	Mean	Std	Min	Max	Mean	Std	Max
Great South Channel Experiment (WHOI/USGS)																						
NA	40°49.0′	69°00.0′	30 March 1976	10 July 1976	101	78	57	7.8	1.6	5	11	−1.0	14.1	−34	38	5.0	43.3	−94	99	41.9	18.5	99
NB	40°51.2′	69°01.2′	14 December 1979	27 May 1980	164	82	67	5.8	1.4	4	10	−2.2	18.3	−51	38	2.3	44.2	−109	100	44.4	18.2	116
M1	40°50.8′	68°48.5′	29 September 1978	19 March 1979	171	66	10	8.5	3.8	3	14	−1.1	23.0	−64	53	4.5	56.0	−114	118	56.9	21.2	120
M2	40°50.7′	68°47.8′	29 September 1978	31 January 1979	124	66	51	10.2	2.9	5	14	−0.4	17.7	−44	43	4.0	47.1	−114	100	47.5	17.1	114
N1	40°50.8′	69°01.0′	31 August 1978	19 December 1978	109	81	10	12.8	2.0	7	18	−4.4	26.1	−76	58	11.2	55.5	−116	125	58.1	22.8	126
N2	40°50.8′	69°01.0′	31 August 1978	30 January 1979	152	81	42	10.6	3.1	5	15	−3.8	23.6	−59	49	8.6	54.8	−109	143	55.7	23.5	145
N3	40°50.8′	69°01.0′	31 August 1978	30 January 1979	152	81	76	10.4	2.9	5	14									43.5	18.2	98
O2	40°52.0′	69°11.0′	2 September 1978	29 January 1979	149	64	27	10.3	3.1	5	14	1.0	23.0	−52	52	−0.3	46.9	−114	99	48.4	19.8	120
O3D	40°52.0′	69°11.0′	2 September 1978	29 January 1979	149	64	49	10.3	3.1	5	14	−1.1	22.3	−54	44	1.1	38.4	−85	84	41.2	16.5	98
Georges Bank Recirculation Experiment (NMFS)																						
11C	40°50.0′	69°19.0′	24 April 1985	1 May 1985	7	40	10	6.8	0.1	7	7	0.4	34.1	−65	59	−14.0	40.6	−80	60	51.7	17.8	88
21A	40°51.0′	69°10.0′	24 April 1985	21 July 1985	88	62	10	9.1	1.7	7	15	−0.2	30.0	−69	63	−4.7	54.7	−112	98	58.7	21.8	126
21B	40°50.0′	69°10.0′	27 August 1985	27 September 1985	31	64	10	14.6	1.3	12	19	−2.4	26.7	−59	63	−4.4	48.7	−104	97	50.7	23.2	114
22B	40°51.0′	69°10.0′	27 August 1985	19 November 1985	83	59	29	13.8	0.9	9	17	−1.2	18.6	−46	52	−0.2	41.5	−91	84	40.4	20.8	93
23A	40°51.0′	69°10.0′	24 April 1985	14 June 1985	50	59	46	7.9	0.8	7	9	−0.6	18.1	−40	41	−3.1	43.5	−101	81	43.7	17.7	108
31C	40°51.7′	68°46.4′	24 April 1985	22 November 1985	211	70	10	12.4	2.8	6	17	−3.9	23.0	−67	53	4.4	49.2	−113	122	50.8	20.1	124
31C	40°52.4′	68°46.0′	29 April 1986	17 November 1986	201	66	10	12.1	2.6	7	17	−3.0	25.7	−72	56	4.4	51.0	−101	99	54.5	18.0	102
32C	40°52.0′	68°47.0′	24 April 1985	9 May 1985	15	70	30	6.7	0.3	6	7	0.2	20.7	−46	41	1.8	52.8	−104	95	52.9	20.3	105
41C1	40°53.0′	68°31.0′	24 April 1985	22 May 1985	27	40	10	7.5	0.7	6	9	−6.0	33.8	−66	63	2.5	54.9	−101	96	62.7	16.1	103
41C2	40°53.0′	68°31.0′	26 July 1985	20 November 1985	116	40	10	14.7	1.1	13	17	−9.8	32.9	−74	63	1.8	55.3	−103	104	62.5	18.3	105
51C	40°44.0′	68°28.0′	24 April 1985	19 November 1985	209	58	10	12.4	2.8	7	20	−18.3	31.5	−98	70	−3.9	51.4	−131	125	58.4	23.8	148
2C	40°44.0′	68°28.0′	24 April 1985	19 November 1985	209	58	28	11.6	2.5	6	21	−11.3	25.0	−68	52	−2.2	43.9	−100	99	48.8	17.2	105
53C	40°44.0′	68°28.0′	24 April 1985	19 November 1985	209	58	45	11.4	2.4	6	16	−7.7	22.5	−78	45	−1.9	39.2	−104	95	42.8	16.6	105
61C	40°29.0′	68°20.9′	29 April 1986	1 October 1986	180	99	10					−11.5	27.3	−86	72	−6.6	32.4	−96	79	41.5	15.9	97
62C	40°29.0′	68°21.0′	25 April 1985	20 November 1985	209	100	30	12.7	4.6	6	23	−14.4	21.2	−83	45	−2.5	28.3	−75	73	35.1	15.3	91
63C	40°29.0′	68°21.0′	25 April 1985	14 September 1985	142	100	50	11.6	1.7	9	19									33.9	14.1	77
64C	40°29.0′	68°21.0′	25 April 1985	20 November 1985	209	100	86	11.3	2.0	7	16	−7.7	17.9	−76	40	−3.8	26.2	−112	70	30.0	13.3	112

Notes: Mooring M was deployed about one month after N and O and retrieved later. N1 (10 m) failed in mid-December, O1 (10 m) never functioned, and N3 (76 m) returned suspect compass values. The 1985 deployment also encountered problems. Instrument 11C (10 m) failed after one week. The surface instrument at site 2 (10 m) had to be redeployed twice due to fishing activity, and that at site 4 (10 m) had to be redeployed once. The subsurface instrument 32CA (30 m) and its 41″ float were recovered afloat by a fisherman on the northeast corner of Georges Bank on 22 May 1985. The instrumented surface mooring deployed at site 6 was never found. One of the three subsurface instruments 63C (45 m) had bad compass readings. The moorings at site 7 (not shown in Fig. 1 and Table 1) were deployed offshore of mooring 6, but the instrumented surface mooring (10 m) was lost. The subsurface mooring at site 7 was found by the British Royal Navy drifting "somewhere in the North Atlantic", however, the current meter data never passed the early stages of processing due to a parity error reading the tape. The 1986 deployment also encountered problems. Mooring 2 (10 m) was lost. Mooring 5 (10 m) never passed the early processing stage due to bad clock values. The subsurface mooring 3 was found floating several miles east of the deployment site on 21 May 1986 with one current meter attached. Despite all these problems, however, the majority of the instruments were recovered and several months of clean data were obtained by each instrument.

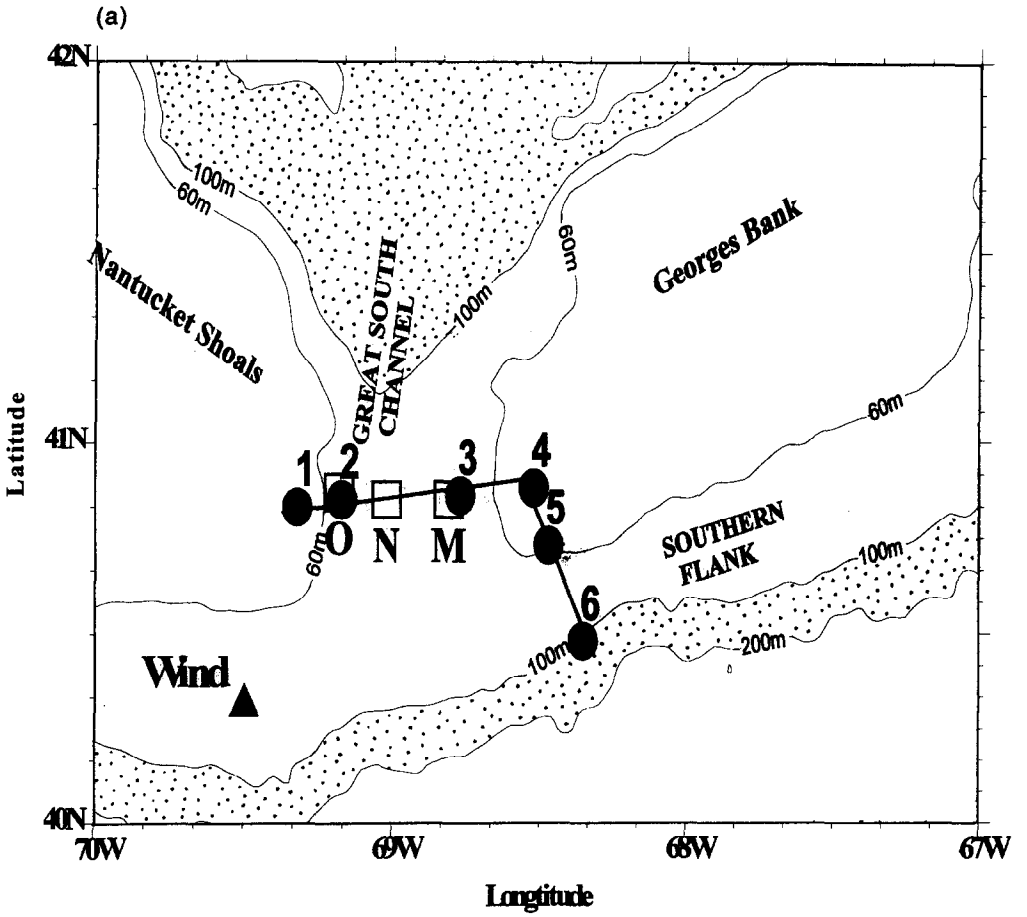

Fig. 1. (a) Mooring locations for WHOI/USGS deployments at sites M, N, and O (denoted by squares) and NOAA/NMFS deployments at sites 1–6 (denoted by circles). The position of the Nantucket Lightship is denoted by a triangle. The NOAA environmental buoy 44008 is located several kilometers west of that location. (b) Instrument configuration for the 1985 NOAA/NMFS deployment in the GSC. Instrument depths within the water column are listed in italics next to the instrument names. The moorings at site 7, located offshore from mooring site 6, did not return useful data, so site 7 is not shown here or listed in Table 1. (See Table 1 footnote for more information about difficulties experienced at site 7.)

METHODS

Correcting biofouled records

Some of the VACMs deployed from April to November 1985 came on deck fouled with rotors not turning easily. Comments on the recovery logs were "rotor turns but stiff", "moderate growth on recovery but still turning", "heavily biofouled, rotor not turning well", etc. The following approach was used to detect the onset of biofouling and then "correct" the current record.

The dominant tidal current in the GSC region is the M2 constituent with a period of 12.42 h (Moody *et al.*, 1984). The M2 tidal kinetic energy of the first 28-day period was

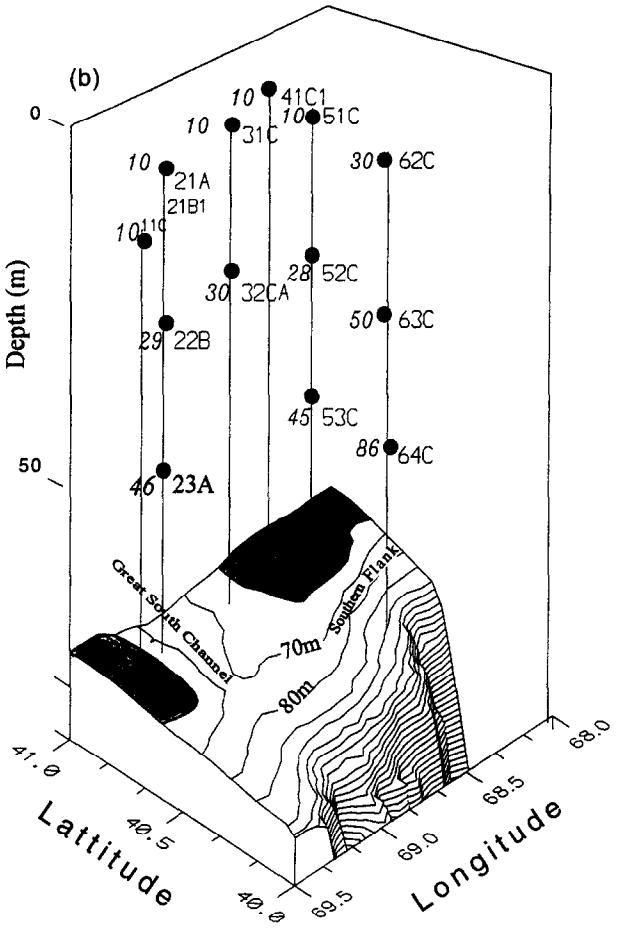

Fig. 1b.

calculated from the basic hourly time-series using the Godin least-squares method (Foreman, 1978) and was then compared with the M2 tidal kinetic energy of each subsequent 28-day period. If there was a decrease in the tidal energy greater than the 95% confidence limits, the subsequent current records were scaled by the factor sqrt (M2 kinetic energy in 1st period)/sqrt(M2 kinetic energy in subsequent period). Different scaling factors were applied to each 28-day period according to the ratio of M2 tidal energy. Six of the 16 records from the 1985 deployment were corrected by this method.

Calculating wind stress

Wind stress was computed from lightship and buoy wind data using the neutral drag law of Large and Pond (1981) with a log-layer correction for anemometer height (which varied from 5 to 17 m above mean sea surface). Basic statistics for the estimated wind stress are listed in Table 2 for each month.

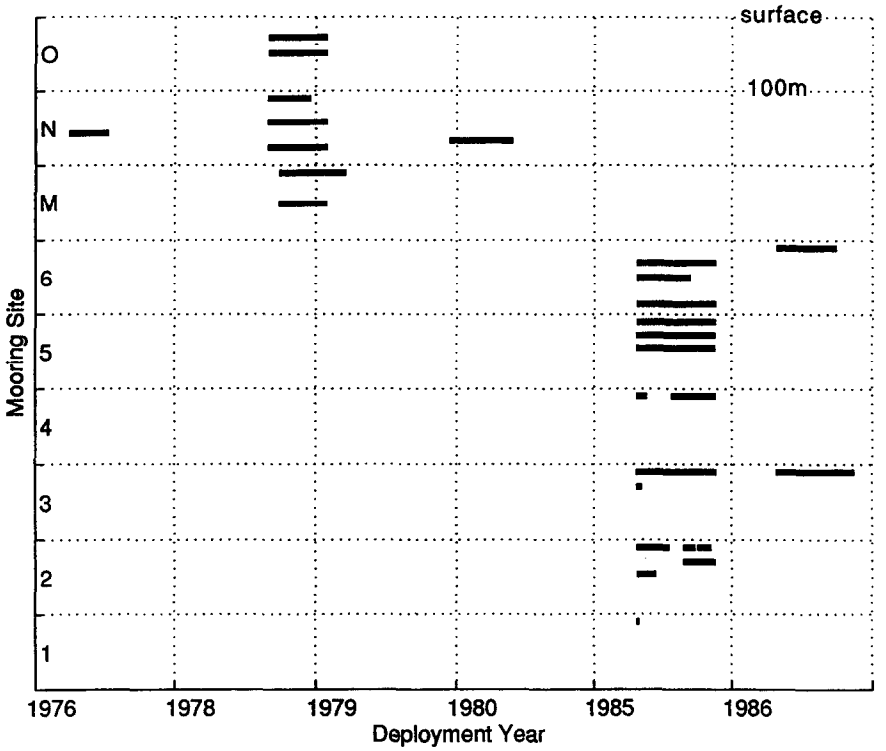

Fig. 2. Bar chart of deployment period and instrument depths. The first major deployment occurred in the autumn–winter months of 1978–1979 and the second major deployment occurred in the summer–autumn of 1985. Bars appear relative to the instrument's position in the water column.

Table 2. Monthly mean wind stress statistics based on a 17-year record from an NOAA buoy in the vicinity of the Great South Channel

	Eastward (Pascals)				Northward (Pascals)				Speed	Dir (to)
Month	Mean	Std	Min	Max	Mean	Std	Min	Max	Mean	Mean
1	0.054	0.143	−0.407	0.814	−0.034	0.116	−0.593	0.386	0.064	122.1
2	0.038	0.127	−0.387	0.587	−0.024	0.113	−0.660	0.373	0.046	122.3
3	0.029	0.125	−0.431	0.546	−0.024	0.104	−0.485	0.385	0.038	129.1
4	0.015	0.077	−0.300	0.329	−0.003	0.075	−0.347	0.259	0.015	102.1
5	0.002	0.046	−0.159	0.147	0.005	0.070	−0.259	0.459	0.005	26.8
6	0.010	0.037	−0.156	0.131	0.010	0.043	−0.175	0.156	0.015	45.2
7	0.009	0.030	−0.136	0.150	0.013	0.036	−0.121	0.143	0.016	33.9
8	0.005	0.051	−0.200	0.375	0.004	0.059	−0.444	0.212	0.007	51.3
9	0.000	0.049	−0.173	0.213	−0.008	0.063	−0.273	0.227	0.008	179.0
10	0.015	0.093	−0.344	0.437	−0.019	0.091	−0.463	0.281	0.024	141.5
11	0.044	0.116	−0.287	0.544	−0.019	0.098	−0.463	0.287	0.048	112.6
12	0.060	0.132	−0.346	0.569	−0.037	0.121	−0.569	0.369	0.071	122.1

Table 3. M_2 tidal current, principal axes, and low-frequency current statistics

	M_2 Tidal Current			%	Subtidal Axes			Low-Frequency Stats			
	Major	Min	Angle	Var.	Major	Min	Angle	U	Std (U)	V	Std (V)
NA	56.3	−15.9	6.7	82	5.3	2.1	16.2	−0.99	2.48	4.98	5.11
NB	56.9	−19.3	11.6	79	9.2	2.8	26.5	−2.15	4.79	2.42	8.29
M1	69.6	−28.0	3.5	77	8.1	5.3	18.0	−1.05	5.65	4.42	7.88
M2	59.4	−22.1	−2.0	79	7.6	2.6	21.1	−0.43	3.66	4.16	7.12
N1	71.6	−26.7	10.3	78	9.6	6.9	56.1	−4.60	8.88	11.34	7.86
N2	74.7	34.7	−18.9	95	10.0	6.0	21.5	−3.72	6.91	8.75	9.93
O2	62.0	−20.6	19.9	78	8.2	2.8	23.9	1.00	4.19	−0.25	7.60
O3	53.3	−17.2	25.0	79	7.0	3.2	27.1	−1.05	4.26	1.12	6.40
211	75.4	−27.1	21.9	82	6.0	2.3	39.9	−0.22	4.21	−4.82	4.81
212	65.7	−24.5	19.2	80	7.4	5.3	40.4	−2.70	6.25	−4.96	6.58
22	56.6	−17.7	16.0	85	6.0	3.5	20.7	−1.30	3.90	−0.25	5.77
23	59.8	−18.2	15.3	88	4.8	1.7	12.2	−0.54	1.95	−3.25	4.69
31	62.2	−26.4	−7.2	77	5.8	4.8	48.9	−3.92	5.39	4.37	5.26
316	70.9	−32.0	−10.7	93	6.1	3.6	46.1	−3.02	5.01	4.48	4.92
32	70.8	−27.4	−6.2	90	4.6	1.3	53.6	0.29	2.89	0.70	3.75
411	75.3	−43.2	−14.4	91	4.7	2.1	47.8	−6.45	4.39	2.32	2.62
412	76.5	−41.6	−13.7	92	4.5	2.4	68.6	−10.00	4.25	1.79	2.75
51	70.5	−35.0	−16.6	85	9.0	4.5	73.6	−18.46	8.77	−4.00	5.05
52	61.7	−29.4	−15.4	92	5.3	2.9	70.7	−11.40	5.12	−2.00	3.29
53	54.2	−25.8	−15.3	88	5.5	2.5	66.2	−7.71	5.09	−1.89	3.21
61	43.1	−28.8	−20.7	75	10.6	5.9	75.1	−9.88	10.40	−5.75	6.33
62	37.4	−22.9	−16.2	77	8.4	5.5	87.2	−14.36	8.38	−2.56	5.56
64	33.9	−19.0	−13.8	75	7.6	3.7	62.5	−7.66	6.93	−3.81	4.77

The current statistics are listed in cm s^{-1}. The orientation angles of the M_2 tidal ellipse and principal axis is clockwise from north. U and V represent the east and north current components.

Current meter analysis methods

In order to examine the subtidal flow field, all current records were low-pass filtered with a 33-h Butterworth filter that essentially removes the diurnal and semi-diurnal tidal components. The principal axes of the low-passed records, along with statistics of the low-passed east/west and north/south velocities, were computed (Table 3). The axis of the GSC is oriented north/south (Fig. 1), so in this region the north/south velocity component corresponds to the along-channel current and the east/west velocity corresponds to the across-channel current. Over the southern flank of Georges Bank, the east/west velocity component corresponds roughly to the along-bank direction and the north/south velocity the cross-bank direction. Coherence and phase were then calculated for both current–current and wind–current relationships. In order to determine the most effective wind direction, wind–current coherences were computed for different wind headings using 15 degree intervals.

Principal component analysis was used to distinguish dominant modes of variability (Morrison, 1967). After removing the mean velocity from the east/west (along-bank) component of the southern flank records and the north/south (along-channel) component of the GSC records, the eigenvectors of the covariance matrix were examined. The time-dependence of these modes were compared to the amplitude of potential forcing (wind and baroclinicity).

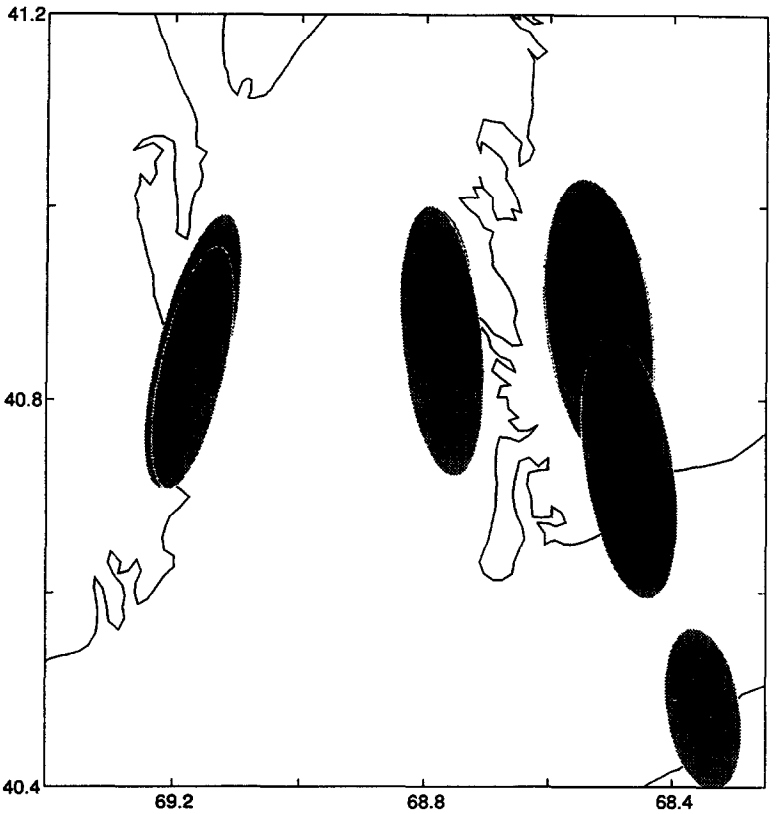

Fig. 3. M2 tidal ellipses for all NMFS surface 10-m deployment periods. See Table 3 for complete listing of all instruments. Note that the two records from site 3 (from 1985 and 1986) give similar results (70 cm s^{-1} major axis) and overlay one another. Similarly for the two deployments at site 4 in 1985.

To examine the degree of recirculation around Georges Bank, the volume transport was calculated for both along-channel flow (from the moorings aligned across the GSC) and the along-bank flow (from moorings aligned across the southern flank). The total transport through each section (Fig. 1a) was estimated as a sum of the weighted current flow; the velocity was multiplied by the representative depth and cross-sectional distance. The instruments positioned closer together in the upper water column were weighted less, therefore, than those in the lower water column. Transport was calculated using hourly data. While the lengths of the transport time series were limited to two-months or less (when enough instruments were in place), they provide a single measure of the along-bank flow that was less affected by the exact cross-shelf location of the current jet over the southern flank of Georges Bank.

RESULTS

The tidal analysis indicates that the M2 constituent is the dominant tidal component and contributes between a minimum of 75% of the total current variability at site 6 (86 m) to a maximum of 95% for instrument N2 (42 m). Typical M2 tidal ellipses are shown for the

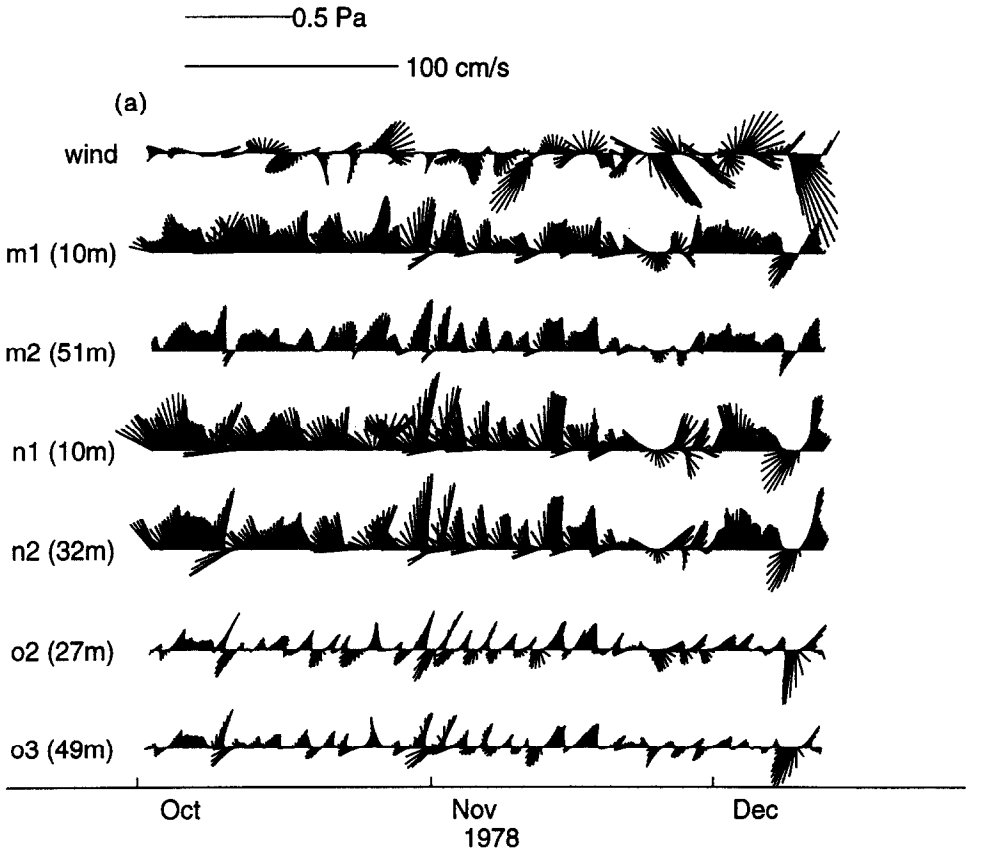

Fig. 4. (a) Stick plot diagram of wind stress (top panel) at the Nantucket Lightship and low-passed filtered currents at sites M, N, and O in fall 1978. North is up. (b) Stick plot diagram of wind stress (top panel) at NOAA buoy 44008 and low-passed filtered currents at sites 2–6 in spring–early summer 1985. North is up.

NMFS deployments in Fig. 3, while tidal ellipses for the WHOI/USGS deployments (which are quite similar in size and orientation) have already been published in Moody *et al.* (1984). As described by Brown (1987), the M2 tide propagates northward through the GSC into the Gulf of Maine, with principal axes oriented roughly parallel with the GSC axis and larger in shallower water. Typical near-surface M2 principal axes along the GSC sill are 56–76 cm s^{-1}. The M2 ellipse statistics for all deployments are included in Table 3 for completeness.

Stick plots of selected low-passed current records and wind stress (Fig. 4) illustrate the general characteristics of the subtidal flow. At the GSC sill sites (M, N, O, and 3), the subtidal flow is dominated by regularly occurring inflow events on timescales of 2–5 days. These events are felt at all depths, particularly on the eastern side, but are seen as far west as site O. While out-channel flow predominates at sites 1 and 2, it is relatively rare at sites M, N, 3, and 4. At the southern flank sites (4, 5, and 6), the flow is less variable in direction and predominately directed towards the southwest, along the local topography. The flow at site 6 is obviously more affected by shelf-slope frontal dynamics than the on-bank sites 4 and 5.

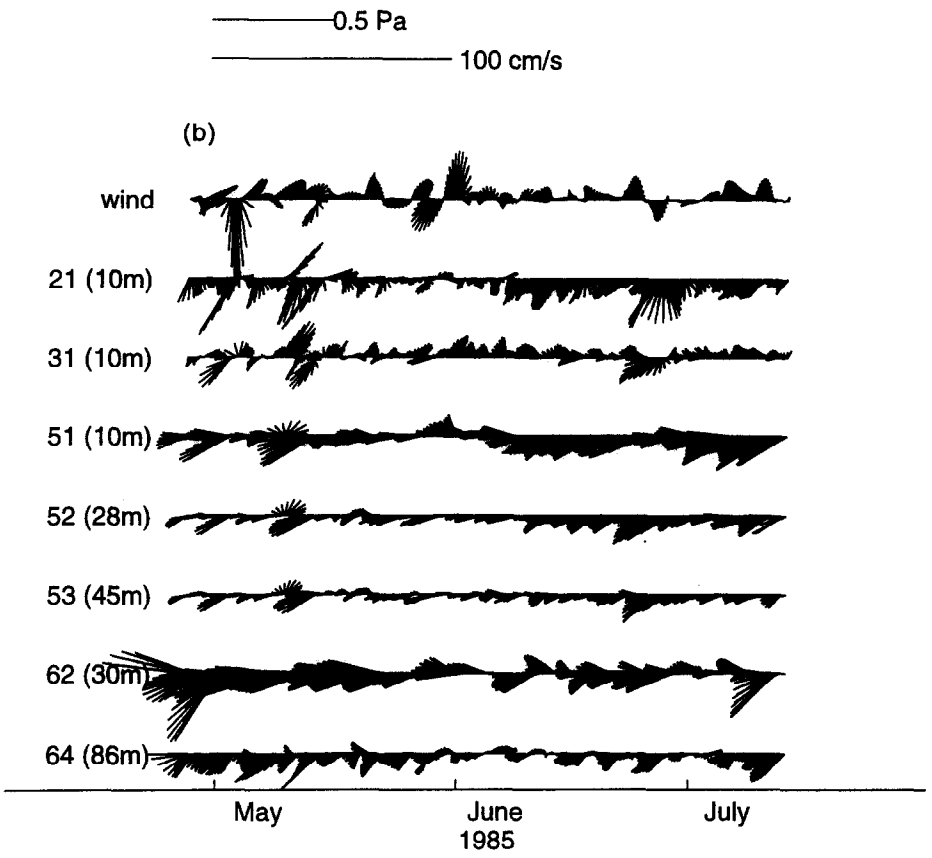

Fig. 4b.

Seasonal variability

Vector plots of all measured monthly mean flow (1976–1986) for the surface (10-m) and deep (30-m and greater) flow (Figs 5a and 5b, respectively) illustrate the degree of spatial and seasonal variability. A strong southward component of wind stress existed from November to March with weaker winds prevailing the remainder of the year and becoming northward in May to August. While very few current meter records (solid arrows) are available from the first months of the year (1–5), those that were in place recorded relatively low flow. Within the GSC (sites 1, 2, 3, O, N, M), the monthly mean currents at all depths are polarized in the along-channel direction, with outflow generally occurring over the western flank of GSC and inflow over the center and eastern flank. Maximum inflows tend to occur in mid-summer through to fall. Over the southern flank, the flow at all depths is strongly polarized in the along-bank direction towards the southwest at site 5 and 6 and primarily west, with a slight northward (recirculating tendency) at site 4.

The principal axes of low-frequency variability were computed for each month of each current record (Fig. 5). Moorings located in deep-water sites recorded larger variability than those in shallower-water sites. The subtidal variability is generally small at site 4, for example, where the water depth is only 40 m. The instruments attached higher in the water

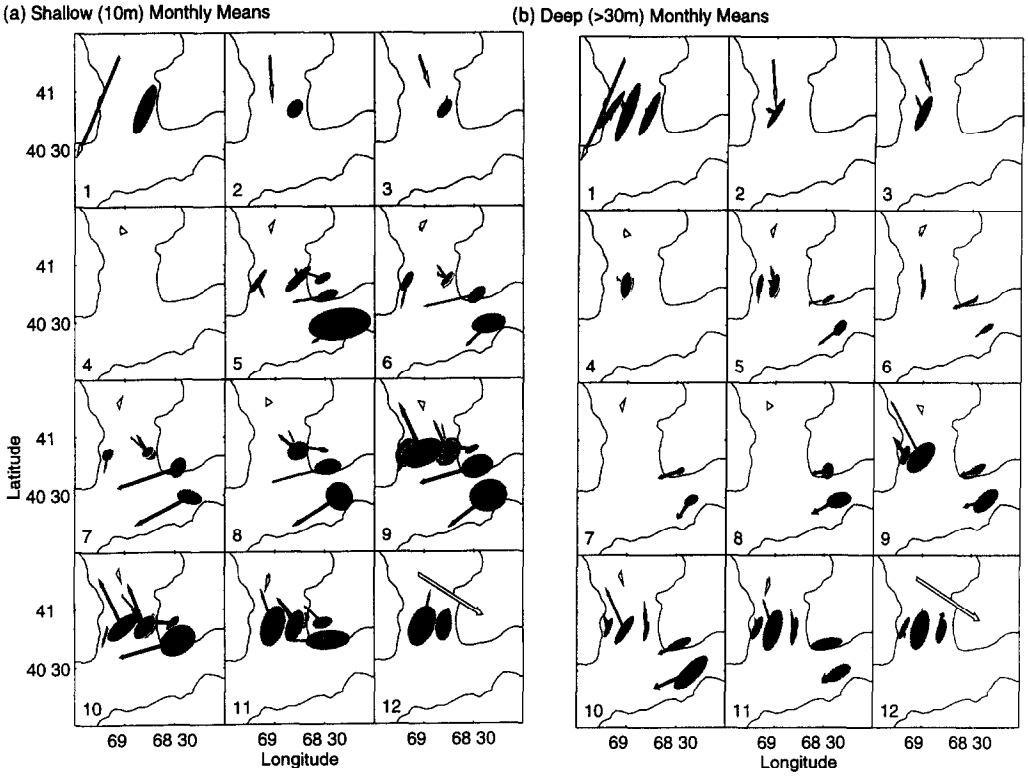

Fig. 5. Monthly mean velocity vectors (solid arrows) for all instruments at (a) 10-m depth and (b) greater than 30-m depth. The values represented by each vector and ellipse may be found in Tables 1–3. Monthly wind stress vectors (open arrows) derived from Nantucket Lightship and NOAA buoy 44008 wind data for the concurrent time periods are included in the upper left corners. The values represented by each vector and ellipse may be found in Tables 1–3. While the number of instruments/samples vary depending on the month, each month is represented by at least one record. The ellipse plotted at the base of each current vector represents the principal axes of subtidal variability (same scale of current vector) as listed in Table 3. The month associated with each panel is displayed in the lower left corners.

column recorded larger variability than those in the deeper part of the water column (Table 3). The principal axis at all depths is oriented a few degrees clockwise of north/south in the GSC, and appears to increase in the winter. At sites 5 and 6 over the southern flank, the orientation of the principal axis is more variable, tending to be more oriented along the local topography at depth and less polarized near the surface.

The monthly mean in-channel flow (Fig. 6) on the western flank of GSC is quite variable in direction, with some tendency for stronger out-channel flow in the summer months. The flow in the center and over the eastern flank of the channel is more consistent in direction, with inflow at sites N, M, and 3 tending to peak with speeds of 5–15 cm s^{-1} in late summer/early fall (September–October).

Current–current relationships

For the 2–10 day low-frequency band, the WHOI/USGS moorings (M, N, and O) indicate higher coherence in the along-channel (north/south) flow than the cross-channel

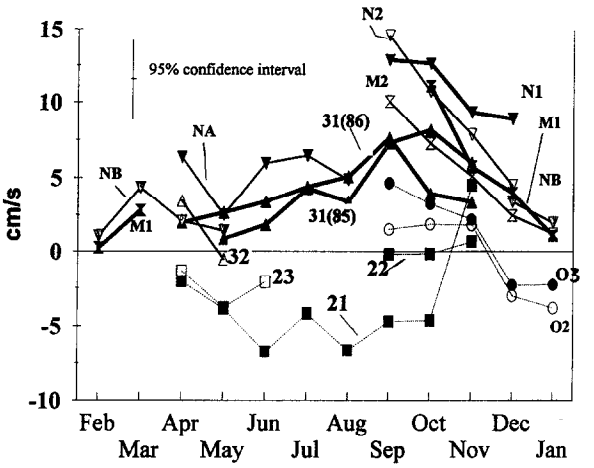

Fig. 6. Monthly mean northward velocities observed at all sites within the GSC. Dashed lines are used for all sites on the western side. Typical confidence interval (± 3.3 cm s^{-1}) is computed as the mean standard deviation of low-passed currents for each month divided by the square root of the equivalent degrees of freedom given a six day decorrelation timescale.

Table 4. Coherence and phase between current meter records

Mooring Number	M1	M2	N2	O2	O3	
M1	1.00 (0)	0.60 (−2)	0.72 (−7)	0.72 (4)	0.61 (−3)	
M2	0.81 (4)	1.00 (0)	0.62 (−7)	0.73 (3)	0.71 (−2)	
N2	0.79 (2)	0.89 (21)	1.00 (0)	0.75 (10)	0.62 (4)	
O2	0.85 (19)	0.91 (15)	0.90 (−6)	1.00 (0)	0.91 (−5)	
O3	0.80 (21)	0.90 (17)	0.87 (−4)	0.97 (3)	1.00 (0)	
Mooring Number	**31**	**51**	**52**	**53**	**62**	**64**
31	1.00 (0)	0.55 (−13)	0.43 (−31)	0.45 (−35)	NS	NS
51	0.29 (−52)	1.00 (0)	0.62 (−15)	0.56 (−23)	NS	NS
52	0.33 (6)	NS	1.00 (0)	0.66 (−14)	0.29 (−30)	NS
53	0.31 (11)	NS	0.36 (−9)	1.00 (0)	0.32 (−24)	NS
62	NS	NS	NS	NS	1.00 (0)	0.37 (16)
64	NS	NS	NS	NS	NS	1.00 (0)

The first array presents coherence and phase results of the WHOI/USGS 1978 and 1979 deployment, and the second array results of the NMFS 1985 deployment. The upper right hand side of each array represents the coherence (degrees) for the E/W flow statistics and the lower right represents the coherence (phase) for the N/S flow. For the upper array, the E/W flow is the cross-channel component, while for the lower array, the E/W flow is the along-isobath component. "NS" stands for not significant at the 95% confidence interval with at least 14 degrees of freedom.

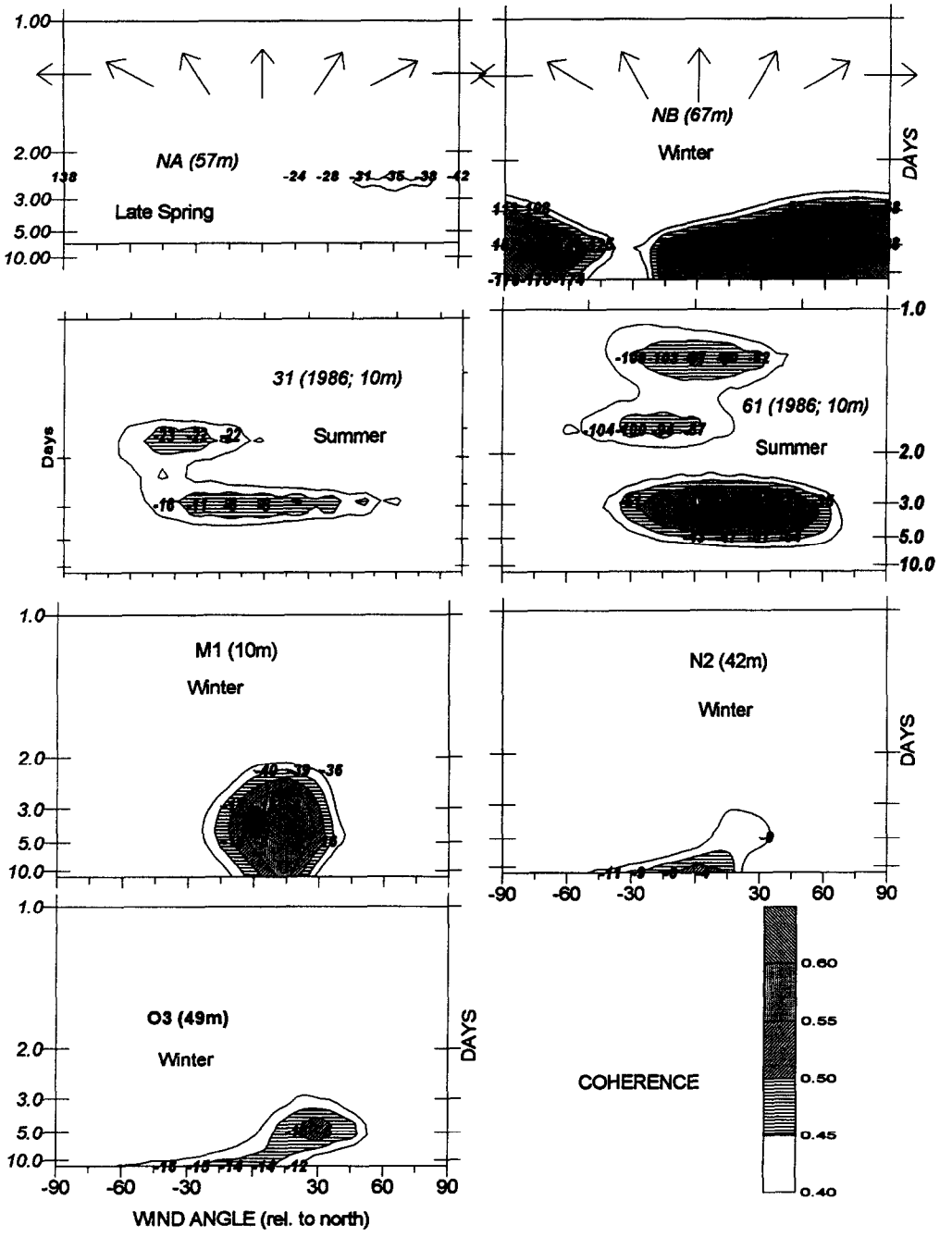

Fig. 7. Wind–current coherence contoured as a function of frequency and wind direction. Wind direction is depicted by the arrows in the top two panels. Phase angle is posted for the significant coherence. The north/south current component was used in each case except at site 6 where the east/west component was used.

surface flow (Table 4: lower left vs upper right). Phase angle, listed along with coherence for each pair, is less than 21 degrees for all WHOI/USGS instruments. A phase angle of positive 21 degrees, for example, between instruments 03 (49 m) and M1 (10 m) indicates that N/S flow at the latter depth leads the former by 21 degrees, which for this 2–10 day band, is equivalent to several hours. The NMFS moorings which were deployed across the GSC at sites 2 and 3 in the opposite time of the year are less coherent.

At sites 4, 5, and 6 over the southern flank of Georges Bank, the along-bank (east/west) flow was more coherent than the cross-bank flow. Phase angles were larger for the NMFS deployment due to the greater separation geographically. For the most significant pairs, however, the lag time is less than a tidal cycle. The flow at site 6 (30 m) is not significantly coherent to other NMFS sites except perhaps the E/W (along-bank) flow at site 5 (28 and 45 m).

Wind–current relationships

The coherence between wind stress and along-channel current at several GSC sites and between wind stress and along-bank current at site 6 were computed for the longer deployments to obtain at least 14 degrees of freedom (using 32 day segments and averaging over four frequency bands; Fig. 7). The coherence data indicate that winds oriented toward the north-northeast/south-southwest are most efficient at driving the along-channel flow, especially during the wintertime deployments (NB, M1). The phase lag between wind and current near this maximum coherence varies from −5 to −40 degrees, indicating that the wind leads the current by less than half a day. During the warmer, more stratified season, the coherence between wind and current is much reduced (note difference in Fig. 7 between 31 (10 m): April–September and M1 (10 m): September–January). At mooring 61(10) in 1986, the along-bank current (3-day periods) was significant with winds rotated anywhere from cross-bank to nearly along-bank. The fact that there was coherence with cross-bank winds indicates probable periods of Ekman transport that drive this along-bank flow in the upper water column (10 m).

A comparison was made (not shown) between the wind stress during the deployment

Table 5. First two principal components of subtidal velocity structure

Run No.	Time Period	Instruments	Mode No.	% Var.	Eigenvector
78	September–October 1978	M1,M2,N1,N2,O2, O3	1	85	.4,.3,.5,.5,.4,.3
			2	8	.7,.3,−.4,−.4,.1,.1
7879	September 1978–January 1979	M1,M2,N2,O2,O3	1	90	.4,.4,.6,.5,.4
			2	6	−.8,−.3,.6,.2,.2
85a	April–August 1985	51,52,53,62,64	1	46	−.4,−.2,.0,.9,.3
			2	40	.7,.4,.3,.2,.4
85b1	April–November 1985	51,52,53,62,64,	1	49	.6,.4,.4,.3,.4,.3
			2	28	.4,.1,.0,−.8,−.3,.2
85b2	April–August 1985	51,52,53,62,64,31	1	43	−.4,−.2,.0,.9,.3,.1
			2	36	.7,.4,.3,.2,.4,.1
85C	April–July 1985	51,52,53,62,64,31,21a	1	50	.5,.2,.1,−.8,−.2,.0,.2

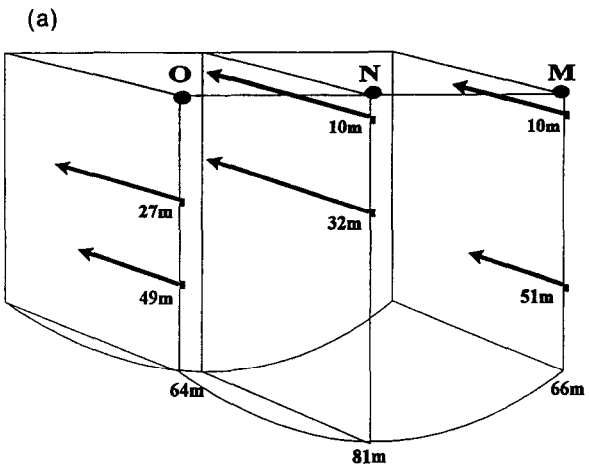

1st Mode (85% of Variance)

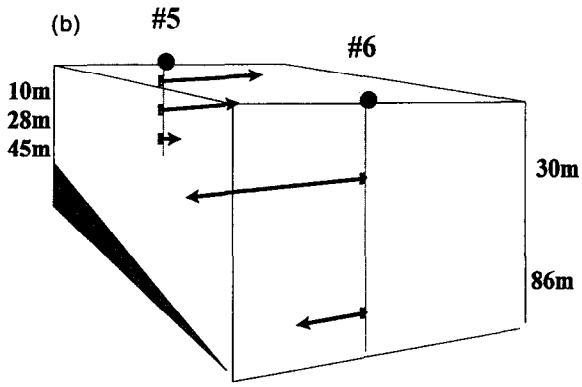

1st Mode (46% of Variance)

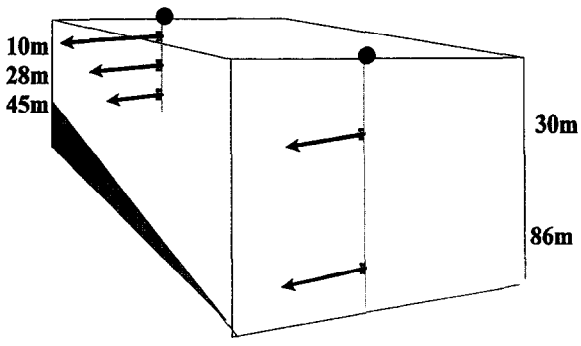

2nd Mode (40% of Variance)

Fig. 8. (a) First principal mode of subtidal variability in the GSC during September–December 1978. (b) First two principal modes of subtidal variability over the southern flank during April–August 1985.

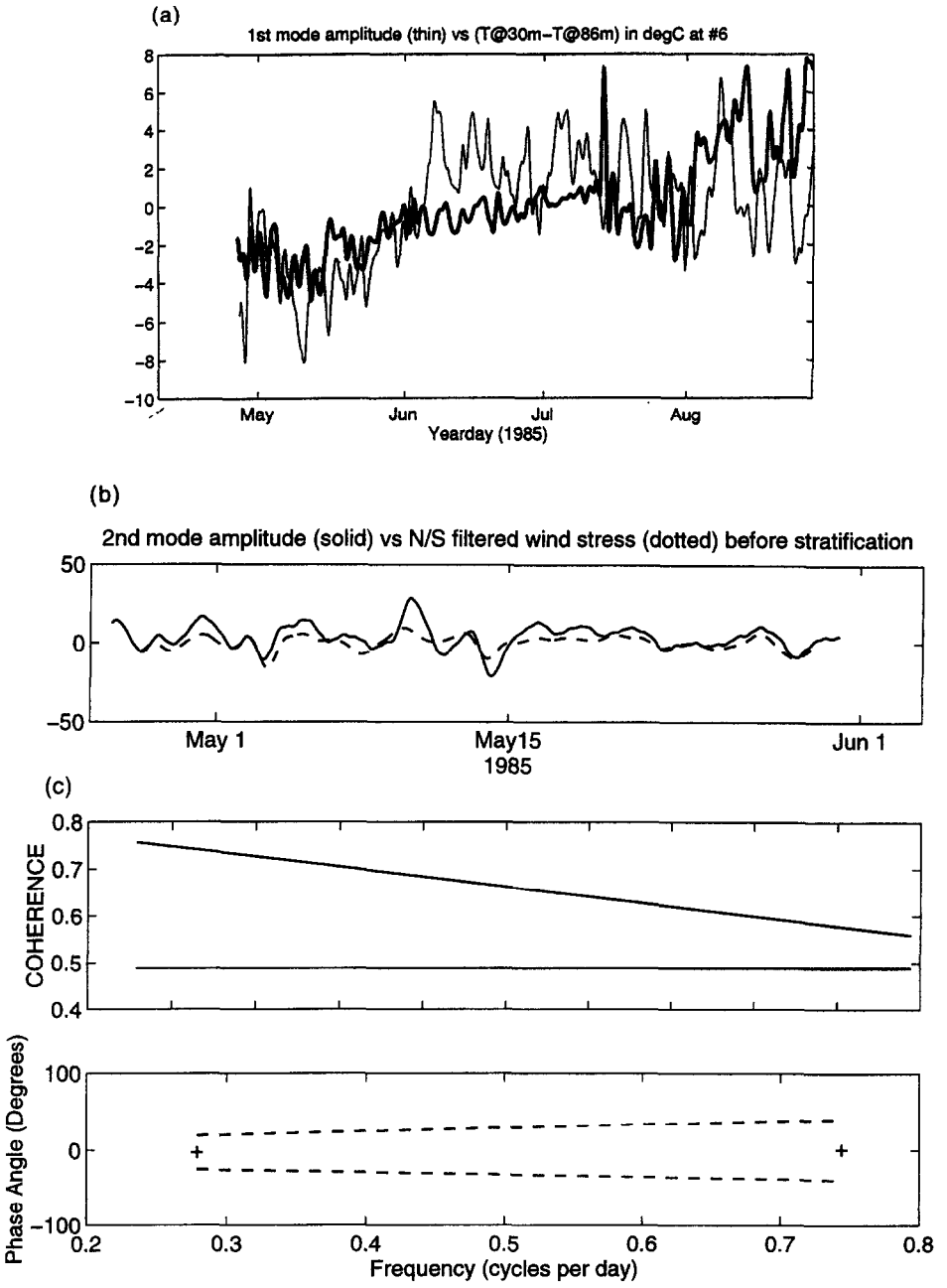

Fig. 9. (a) Amplitude of first southern flank mode and temperature difference between instrument 62 (30 m) and 64 (86 m). (b) Amplitude of second southern flank mode and east–west wind stress at NOAA buoy 44008 before the onset of stratification. (c) Coherence and phase of second southern flank mode with east/west wind stress before the onset of stratification. Note because of the shortness (35 days) of the record, coherence and phase estimates computed with 12 degrees of freedom were centered at 3.6 and 1.3 days. Only two frequencies are shown.

periods and a "historical" 17-year wind-stress record (Table 2) to check if anomalous conditions existed during the deployment periods. The most obvious anomalies are stronger than normal winds during February 1979 (when mooring M1 was the only instrument deployed) and the winter of 1979–1980 (when mooring NB was the only instrument deployed). These two instruments (M1 and NB) showed the highest coherence with wind (Fig. 7).

Modes of variability

In order to visualize the spatial structure of the low-frequency flow, empirical orthogonal modes of subtidal current variability were computed for several different time periods (Table 5). The dominant mode of subtidal variability in the GSC during autumn–winter 1978–1979 (case 7879) was coherent along-channel flow at all measurement sites (Fig. 8a). This model accounted for more than 85% of the subtidal variability and is coherent with the rotated wind stress as in the individual record discussed above.

Over the southern flank at sites 5 and 6 during the 1985 April–August period (case 85a), two modes were dominant. The first mode (Fig. 8b) shows that increases in along-bank velocity at the outer-shelf site 6 (100 m water depth) are associated with a simultaneous slow-down in along-bank flow at the mid-shelf site 5 (58 m water depth). This mode explains 46% of the overall variance in the April–August period and may be related to either the onset of stratification, the foot of the shelf-slope front impinging onto the bank, or both. Note that the amplitude of the mode changes sign simultaneously with the sign of vertical stratification near the end of May. The amplitude of this mode is plotted in Fig. 9a along with the degree of thermal stratification as measured at site 6. (Note that this measure of stratification includes both shelf-slope front effects as well as surface warming.) The second mode (which explains 40% of the subtidal variance during this period) depicts a coherent increase or slow-down at all instruments (Fig. 8c) that appears to be driven by the wind, especially before the onset of stratification (Fig. 9b). Significant coherence of mode 2 was computed for winds rotated from NNW to ENE, but given the short pre-stratification

Table 6. Estimates of subtidal volume transport through the GSC and along the southern flank. Positive transports mean northward in-channel flow in the GSC and westward along-bank flow over the southern flank

Time Days	Period (no. days)	Transport (Sv)	Instruments Used	Per Inst. Vertical Distance (m)	Per Mooring Lateral Distance (km)	Total Lateral Distance (km)
In-channel						
24 April–8 May 1985	14	0.031	21A,23A,31C,32,41C1	30,30,20,50,40	19.9,22.0,13.2	55.1
29 August–6 November 1985	69	0.095	22B,31C,41C2	40,70,40	19.9,11.0,13.2	55.1
1 September–31 October 1985	61	0.106	22B,31C,41C2	40,70,40	19.9,11.0,13.2	55.1
1 September–31 October 1985	61	0.113	31C,41C2	70,40	22.0,13.2	35.2
29 September–19 March 1978	169	0.115	M1,M2,N1,N2,O2,O3	35,35,20,50,15,30	10.6,7.9,7.4	25.9
31 August 1978–19 March 1979	137	0.078*	M1,M2,N1,N2,O2,O3	35,35,20,50,15,30	10.6,7.9,7.4	25.9
South flank						
27 July–18 November 1985	112	0.421	41C2,51,52,53,62,64	40,19,17,22,40,60	11.3,19.4,16.2	46.7
1 September–31 October 1985	61	0.428	41C2,51,52,53,62,64	40,19,17,22,40,60	11.3,19.4,16.2	46.7

*This estimate was obtained using the mean velocity of the full record of each instrument.

period, only 12 degrees of freedom were obtained. If data from sites 2 and 3 are included (cases 85b2, 85c), then the basic structure of the lowest two dominant modes does not change over the southern flank, but the relative importance of the two modes does depend on the degree of stratification.

Volume transport

The volume transport through the Great South Channel was calculated for periods when there was adequate coverage (see Table 6). The mean transport was 0.031 Sv for the 1985 late spring period (positive transport means northward in-channel flow). The mean transport was 0.095 Sv for the longer 1985 autumn period. While there were no instruments operating in the lower half of the water column at site 3 during this period, it was possible to derive a transfer function between upper and lower layer flows there given the observations at site M in 1978–1979. The deeper instrument (M2) recorded subtidal velocities at 0.79 times the surface instrument (M1). This figure was used to adjust the deeper flow at site 3 in 1985 and therefore provide a better estimate of transport in the lower portion of the water column (40–70 m). During autumn 1978, three sites were occupied across the channel, with the middle site, N, being in the axis of the channel and recording stronger flows (see Fig. 6) than measured over either flank at M and O. Two estimates of transport were made for this autumn 1978 period. The first estimate, using only those times when all instruments were in the water, resulted in 0.115 Sv, and a second estimate of 0.078 Sv was obtained using the mean velocities of the complete instrument records. Both of these are close to the autumn 1985 estimate discussed above despite the smaller cross-sectional distance.

The mean westward transport along the southern flank of Georges Bank estimated from

Table 7. Per cent recirculation

Kilometers Across GSC							
60	50	40	30	20	10		
724	368	193	91	42	19	10	Kilometers
348	177	93	44	20	9	20	Across the
168	85	45	21	10	5	30	Southern
82	42	22	11	5	3	40	Flank
41	21	11	6	3	2	50	
21	11	6	3	2	1	60	

Note: Per cent recirculation calculated using 10 km increments of each transect across the GSC and southern flank, respectively. In both transects, three moorings were available to estimate transport. In order to make estimates of transport for each 10 km segment, the weighting vectors [.8 .7 .5 .1 .0 .0 .0], [.2 .3 .5 .8 .5 .3 .2], and [.0 .0 .0 .1 .5 .7 .8] were used for the on-bank, mid-section, and off-bank instruments, respectively. This exercise was conducted for the autumn 1985 deployment using the top 40 m only. For example, 93% of the flow through the first 20 km of the southern flank transect flows through the first 40 km of the GSC transect.

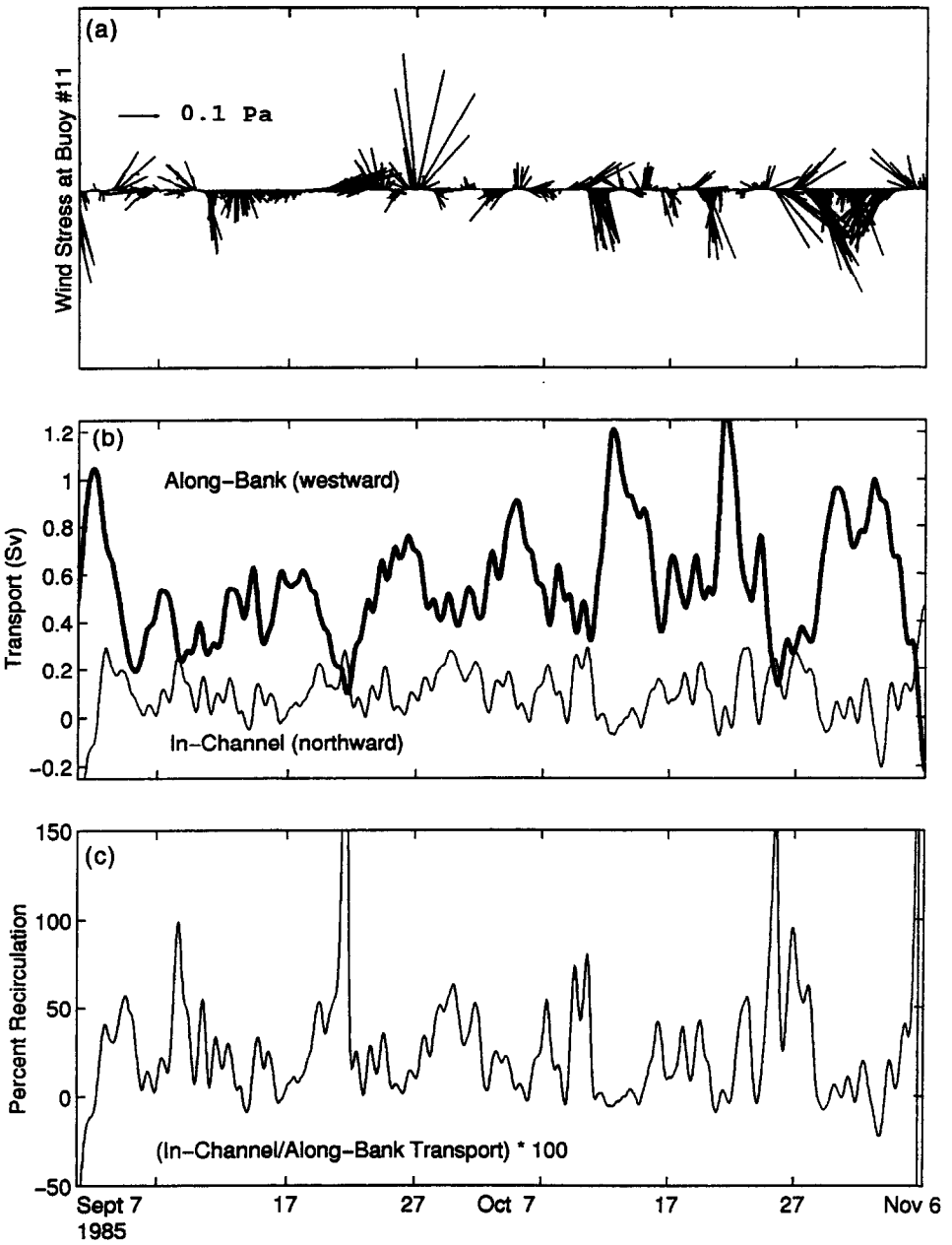

Fig. 10. Time-series of wind stress at NOAA buoy 44011 (a), along-bank and in-channel transports (b), and per cent transport from southern flank recirculating around Georges Bank through the GSC (c) in autumn 1985.

measurements made at site 4–6 was 0.428 Sv for September–October 1985. Thus 25% of the along-bank transport between the 40- and 100-m isobaths on the southern flank turned northward through the GSC to recirculate around Georges Bank in September–October 1985. Butman and Beardsley (1987a) estimate of "on the order of perhaps 50% in summer

and 25% in winter" is slightly higher than the estimates made here. The small discrepancy may be due in part to our lack of current information in the deeper portion of the channel near the 70 m isobath where much of the recirculation could potentially occur. Our estimates for autumn 1985 used data from the NMFS sites 2–4 which did not cover the axis, where the strongest currents were observed at site N during the WHOI/USGS deployments.

The exact value of "per cent recirculation" depends, of course, on the definition of the geographic transects. In order to examine this in more detail, an estimate of transport was made for each of six 10-km segments both across the southern flank and across the GSC. (Each instrument was assigned an appropriate linear weight for each segment so that the total weights for each segment summed to 1.0, and only the top 40 m of the water column were used in this exercise.) The resultant per cent recirculation matrix is presented in Table 7. Note that the diagonal from upper-right to lower-left represents the per cent recirculation resulting from equivalent cross-sectional segments and that they range from 19–22% depending on how one defines the length of the transect.

In all of the above mean per cent recirculation estimates, simultaneous time series are used. What happens when the transport events are given time to propagate around to the GSC? When the southern flank records were lagged iteratively in 12 h intervals backwards in time for two weeks, the per cent recirculation peaked at approximately 9 days where it ranged from 21 to 25%.

In order to examine the transport variability over time, an hourly transport estimate was generated from the basic low-pass filtered current data. In-channel (northward) and along-bank (westward) transports, and "per cent in-channel flow" (time series derived from the quotient of the two transports) are plotted in Fig. 10. The latter time series indicates a significant amount of variability around the mean value of 19–25% given above. The timescale of variability for the in-channel flow is smaller than that for the along-bank flow (Fig. 10). A curious feature of the along-bank transport is the 8–9 day cycle of variation whose amplitude seems to grow over the two-month period plotted. While there is no visually-apparent correlation with the wind stress time-series shown in Fig. 10, it is possible that the large wind event on 28 September may have induced a freely propagating event. The exact mechanism associated with apparent shelf waves is not addressed here. They have been observed by Noble *et al.* (1985) in this region and by Louis *et al.* (1982) upstream on the Scotian Shelf.

DISCUSSION

Volume transport

How do these observations compare with other reports in the literature? The along-bank transport estimate of 0.42 Sv for autumn 1985 is comparable to the estimate of 0.38 Sv obtained approximately 150 km to the west during the October 1979–March 1980 Nantucket Shoals Flux Experiment (Beardsley *et al.*, 1985). The GSC in-channel transport estimate of 0.095 Sv is in good agreement with recent model simulations by Naimie *et al.* (1994). In an investigation of bimonthly flow fields, they estimate a 0.11 Sv flow northward through the eastern flank of the GSC for the September/October period.

The per cent recirculation estimates of 19–25% for autumn 1985 is slightly lower than the 25–50% noted in Butman and Beardsley (1987a, 1987b), but the later estimate is derived from other years of observations, including measurements at site N which was more

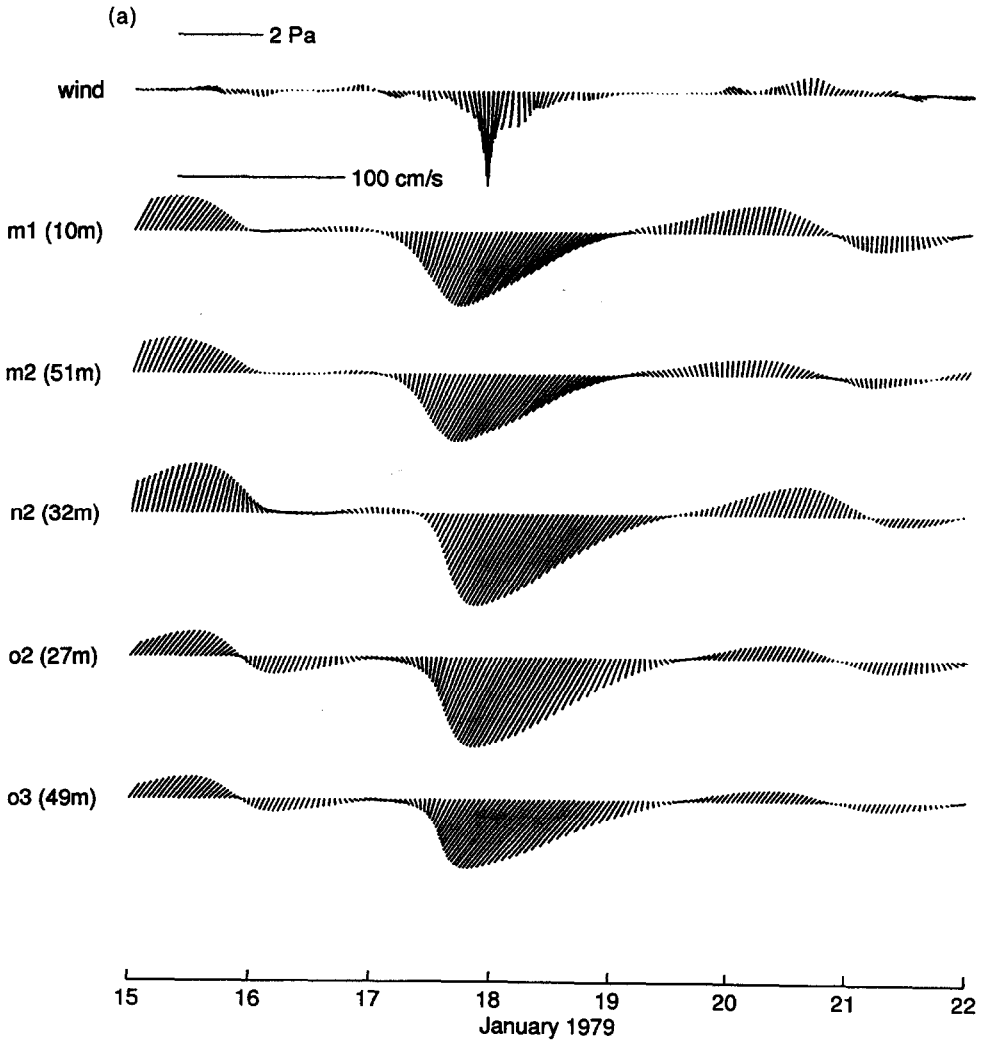

Fig. 11. (a) GSC current response to a strong southward wind event in January 1979. (b) Current response to a strong southward wind event in May 1985. (c) An oscillatory current event in the GSC in November 1978.

centrally located (mid-channel) and may have captured a larger portion of the topographically controlled flow. The calculation of "percent recirculation" is obviously sensitive to the cross-sectional area of the transect. Extensions of the off-bank limit increases the total volume transport dramatically due to the sharp increase in depth contours. Along-bank transport along the edge of the bank is also subject to Gulf Stream ring entrainments and shelf-slope front dynamics.

Wind events

In addition to providing information on the mean flows, these current meter records document the episodic nature of the flow field. While the events we consider next all appear

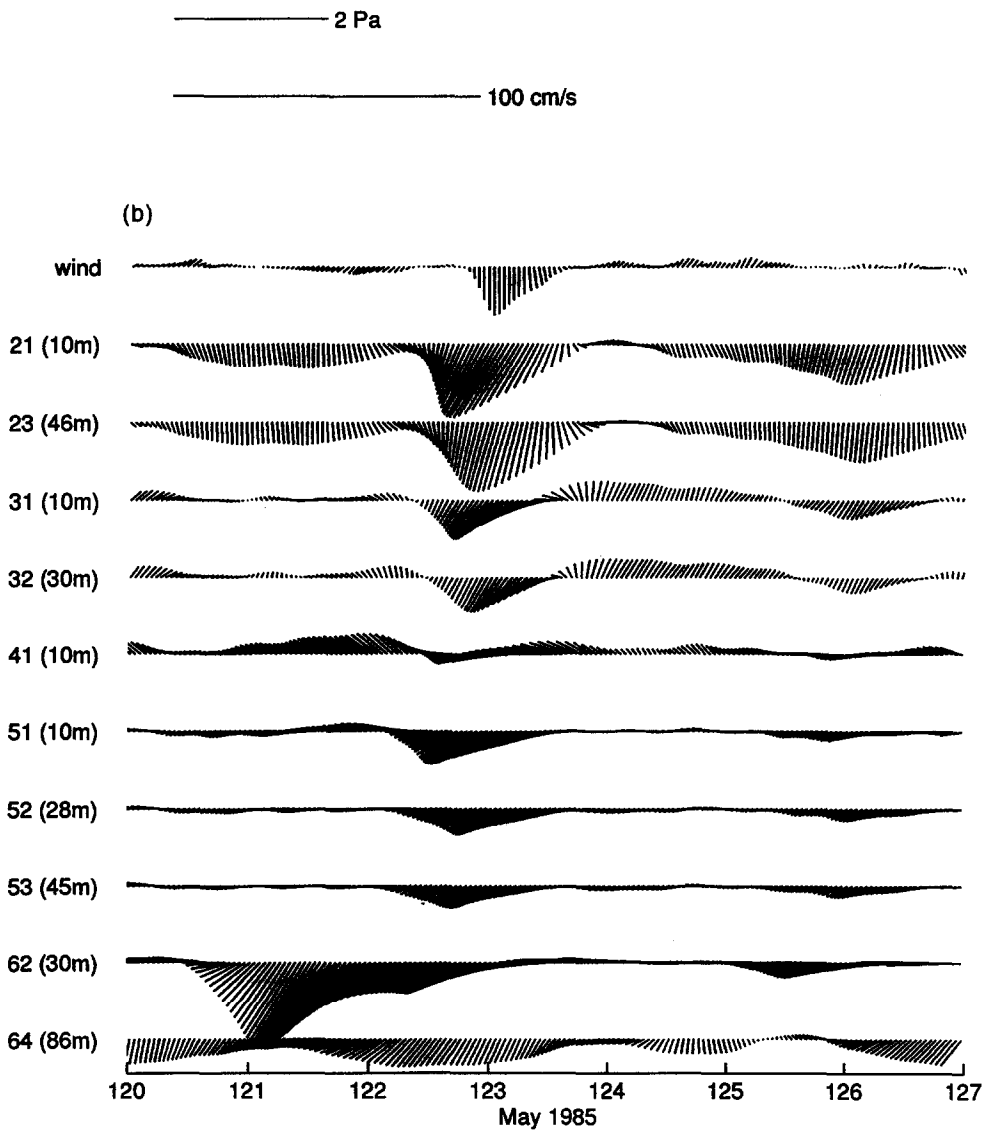

Fig. 11b.

to be primarily driven by the wind, we recognize the importance of other forcings such as the shelf/slope frontal instabilities, coastal-trapped waves, and Gulf Stream ring intrusions.

As depicted in the monthly mean vectors in Fig. 5, the wind stress during the first few months of the year has a strong southward component. How does this influence the current in the GSC region? While the calculations of wind–current coherences presented above did provide evidence for a wind-driven mechanism, only anomalously strong wind events generated highly significant wind–current coherence. It is therefore often more enlightening to focus on a few events where wind is the dominant driving force. Three wind events are considered next, 19 January 1979, 4 May 1985, and early November 1978.

A southward wind stress in excess of 1 Pascal prevailed for several hours in the early

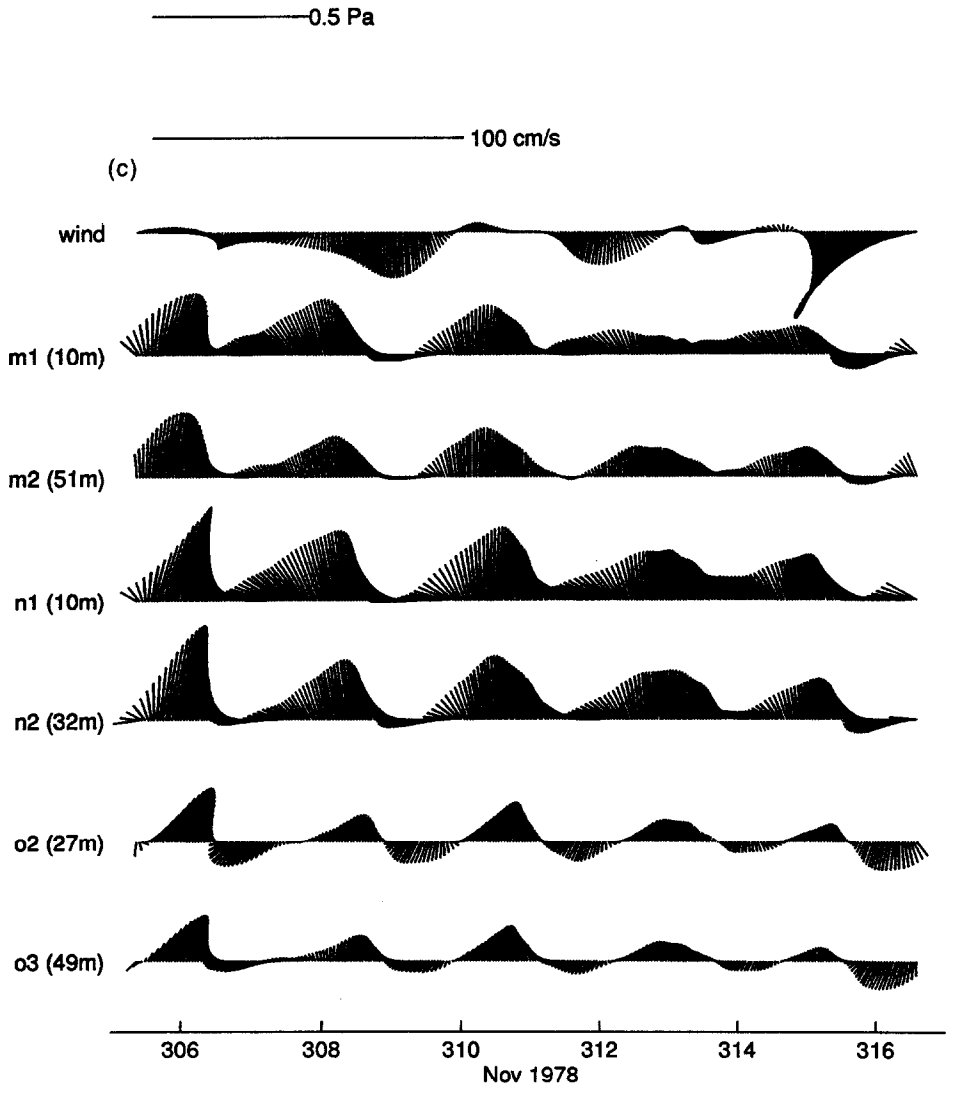

Fig. 11c.

morning of 19 January 1979 (Fig. 11a). The current response to this event was apparent at all three sites across the GSC and resulted in a 30 cm s^{-1} southward sub-tidal current. While the wind stress is not usually strong enough to reverse the mean in-channel flow as it did on this occasion, it probably retards a portion of the tidally-rectified component of flow, especially in these first few months of the year. Another example of this type of wind event occurred on 4 May 1985 (Fig. 11b). The out-channel flow at site 2 was enhanced, the in-channel flow at sites 3 and 4 were reversed, and the along-bank flow at site 5 enhanced essentially in phase with the wind stress forcing. The deeper flow at site 6 appears to be independent of the wind due to the possible dominance of density dynamics in the region of the shelf/slope front.

Lastly, the detided current records in the GSC for the first few weeks of November 1978

contain a roughly sinusoidal oscillation (Fig. 11c). The amplitude of the oscillation is approximately 15 cm s^{-1} and falls off to near zero six cycles later, resulting in a period of approximately 50 h. The filtered wind stress exhibit similar oscillations. While clearly not as regular and dramatic as the current oscillations, close examination indicate that for each episode of southerly wind, the in-channel (northward) current flow is reduced and pushed westerly. Similar two-day current oscillations were observed in January 1980 at NB (not shown).

Shelf-slope front

The current kinetic energy spectrum at the shelf edge site (6) does not exhibit any significant peak near 0.3 cycles day^{-1} as does the spectrum of along-bank wind stress. The dominant subtidal current in this more stratified location is more likely due to density gradients. In an attempt to determine the influence of the shelf/slope front on subtidal current variability over the southern flank, the weekly frontal position from April–November 1985 was taken from Armstrong (1986). Time series plots of frontal positions along the 160° Casco Bay line (roughly parallel to 68°) were generated, but they show no visual coherence with either current mode amplitude or volume transport time series. It should be noted that these frontal positions are surface expressions of the front and may not be an accurate description of the deeper foot of the front. One indicator that the base of the front was inshore of site 6 during this time is that the water at 87 m at mooring site 6 was a few degrees **warmer** than at 30 m for several weeks in May–June 1985 (Fig. 9a).

Biological significance

What do our results infer about the retention or loss of fish larvae on Georges Bank? If the distribution of planktonic larvae are spread out over space and time on the southern flank, a consistent portion (19–25%) will be retained on the bank. However, if the distribution of larvae is patchy, the portion retained on the bank may vary year-to-year. The first empirical mode (Fig. 8b) on the southern flank indicates a cross-bank current structure that may subject on-bank larvae to a very different fate than those on the offbank edge consistent with recent findings in the literature (Werner *et al.*, 1993; Lough *et al.*, 1994). The short term (2–3 day) variability of GSC transport may have significant consequences for free-drifting larvae as they arrive at the entrance to the channel. Consider, for example, a 100 km^2 "patch" of larvae similar to those observed recently on the southern flank (Manning *et al.*, 1995). A typical in-channel transport event of 0.5 Sv in late spring can easily advect that volume of water safely around the southwest corner of the bank in just a few days, but these events are very episodic so that the animal's potential to recirculate may be largely dependent on the chance of their arriving during such an event.

SUMMARY

A compilation of all moored current meter records obtained in the Great South Channel region provides at least some insight to understanding a highly complex flow field regulating Georges Bank recirculation. While the seasonal mean flow increases in spring and summer due to increased stratification and tidal rectification, other equally important forcing processes such as wind and shelf wave phenomenon can have a dramatic effect on day-to-

day subtidal current variations. The wind stress direction most effective in driving in-channel (out-channel) flow in the GSC is oriented north-northeastward (south-southwestward); however, only anomalously strong winds generate significant current forcing. The deeper currents respond to the relatively longer (~10 day) period winds while the near-surface currents respond to the 2–3 day storms, but the response in both cases starts in a matter of hours.

While less than 25% of the transport along the southern flank entered the GSC during a two month period in autumn 1985, subtidal variability of the GSC transport was highly energetic, with the standard deviation (~0.11 Sv) exceeding the mean (~0.095 Sv). The "per cent recirculation" can change from 0% to 100% in just a few days.

Acknowledgements—The authors acknowledge the leadership of R. Schlitz, B. Butman, J. Vermersh, and their co-workers who conducted the field experiments that produced the moored current meter data examined here. A preliminary unpublished analysis of the wind-driven variability in the WHOI/USGS data set was made by Vermersh, which helped guide our analysis. A. M. Michael helped with the preparation of the final manuscript. Support during the analysis and writing of this manuscript was provided by NMFS for Manning and both the NSF Grant OCE93–13671 and WHOI Coastal Research Center for Beardsley.

REFERENCES

Armstrong R. (1986) Variation in the Shelf Water Front Position in 1985 from Georges Bank to Cape Romain, Northwest Atlantic Fisheries Organization Scientifica Council Report Doc. 86/74.

Beardsley R. C., D. C. Chapman, K. Brink, S. R. Ramp and R. Schlitz (1985) The Nantucket Shoals flux experiment. Part I: A basic description of the current and temperature variability. *Journal of Physical Oceanography*, **15**, 713–748.

Bigelow H. B. (1927) Physical oceanography of the Gulf of Maine. *Fisheries Bulletin, U.S.*, **40**, 511–1027.

Brown W. S. and J. A. Moody (1987) Tides. In: *Georges Bank*, R. H. Backus and D. W. Bourne, MIT Press, Cambridge, MA, 593pp.

Bumpus D. F. (1976) Review of the Physical Oceanography of Georges Bank, ICNAF Bulletin Number 12.

Butman B., R. C. Beardsley, B. Magnell, D. Frye, J. A. Vermersch, R. Schlitz, R. Limeburner, W. R. Wright and M. A. Noble (1982) Recent observations of the mean circulation on Georges Bank. *Journal of Physical Oceanography*, **12**, 569–591.

Butman B., M. A. Noble, D. C. Chapman and R. C. Beardsley (1983) An upper bound for the tidally rectified current at one location on the southern flank of Georges Bank. *Journal of Physical Oceanography*, **13**, 1452–1460.

Butman B. and R. Beardsley (1987a) Physical oceanography introduction. In: *Georges Bank*. R. H. Backus and D. W. Bourne, MIT Press, Cambridge, MA, 593 pp.

Butman B. and R. Beardsley (1987b) Long-term observations on southern flank of Georges Bank. *Journal of Physical Oceanography*, **17**, 367–384.

Foreman M. G. G. (1978) Manual for tidal currents analysis and prediction. Pacific Marine Science Report 78–6, Institute of Ocean Sciences, Patricia Bay, Sidney, B.C., 70 pp.

Large W. G. and S. Pond (1981) Open ocean momentum flux measurements in moderate to strong winds. *Journal of Physical Oceanography*, **11**, 324–336.

Lough R. G., W. G. Smith, F. E. Werner, J. W. Loder, F. H. Page, C. G. Hannah, C. E. Naimie, R. I. Perry, M. Sinclair and D. R. Lynch (1994) Influence of wind-driven advection on interannual variability in cod egg and larval distribution on Georges Bank: 1982 vs 1985. *ICES Marine Science Symposium*, **198**, 356–378.

Louis J. P., B. D. Petrie and P. C. Smith (1982) Observations of topographic Rossby Waves on the continental margin off Nova Scotia. *Journal of Physical Oceanography*, **12**, 47–55.

Manning J. P., T. Holzwarth-Davis, M. Taylor, T. Rotuno, D. Mountain and R. Lough (1995) 1995 Georges Bank Stratification Study: 1992 Data Report. Northeast Fisheries Science Center Reference Document Ref. Doc. no. 95–10, 109 pp.

Moody J. A., B. Butman, R. Beardsley, W. S. Brown, P. Daifuku, J. D. Irish, D. A. Mayer, H. O. Mofjeld, B.

Petrie, S. Ramp, P. Smith and W. R. Wright (1984) Atlas of tidal elevation and current observations on the Northeast American Continental Shelf and Slope, USGS Bulletin 1611, Woods Hole, MA.

Morrison D. F. (1967) *Multivariate statistical analysis*, McGraw-Hill, New York.

Naimie C. E., J. W. Loder and D. R. Lynch (1994) Seasonal variation of the three-dimensional residual circulation on Georges Bank. *Journal of Geophysical Research*, **99C8**, 15,967–15,989.

Noble M. A., B. Butman and M. Wimbush (1985) Wind–current coupling on the southern flank of Georges Bank: Variation with season and frequency. *Journal of Physical Oceanography*, **15**, 604–620.

Werner F. E., F. E. Page, D. R. Lynch, J. W. Loder, R. G. Lough, R. I. Perry, D. A. Greenberg and M. M. Sinclair (1993) Influences of mean advection and simple behavior on the distribution of cod and haddock early life stages on Georges Bank. *Fisheries Oceanography*, **2**, 43–64.